



Template-free synthesis of NiO skeleton crystal octahedron and effect of surface depression on electrochemical performance

Dong Huang¹ · Haixia Liu¹  · Tianduo Li¹ · Qingfen Niu¹

Received: 10 November 2018 / Accepted: 15 December 2018 / Published online: 27 December 2018
© Springer Science+Business Media, LLC, part of Springer Nature 2019

Abstract

In this work, we were committed to building a nickel oxide (NiO) octahedron with skeleton crystal structure as a capacitor electrode for supercapacitance through a template-free and efficient one-step process. Initially, nickel nitrate hexahydrate ($\text{Ni}(\text{NO}_3)_2 \cdot 6\text{H}_2\text{O}$) and anhydrous ethanol mixtures were used as a material. The final samples were prepared by calcining the precursor at different temperatures. The mechanism of crystal recrystallization at different temperatures during calcination was discussed. Generally speaking, in the process of rapid growth with only diffusion mechanism, crystal imperfections such as crystal plane depression and skeleton crystal will be formed. At the lower temperature calcination, small depressions are produced due to the effect of crystal face Ostwald ripening. At higher temperatures, the crystal edge growth rate is faster than the surface growth rate during Ostwald ripening and recrystallization, resulting in the formation of NiO octahedron with a large surface depression skeleton crystal structure. The electrochemical test results of the samples showed that the surface depression NiO octahedron has fine supercapacitive behaviors and specific capacitance values (640 F g^{-1}) at the discharging current of 0.5 A g^{-1} in the 3 mol L^{-1} KOH electrolyte and maintain excellent cycling stability, remaining constant after 2000 cycles. Electrochemical impedance measurements confirmed the capacitance performance of NiO electrodes.

Supplementary information The online version of this article (<https://doi.org/10.1007/s10971-018-4908-3>) contains supplementary material, which is available to authorized users.

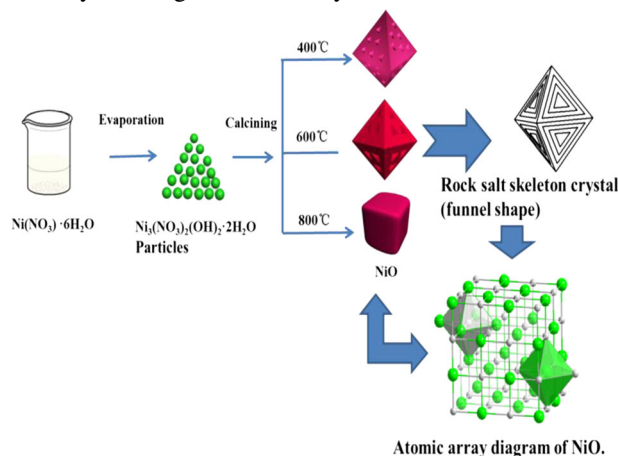
✉ Haixia Liu
liuhaixia929@163.com

✉ Tianduo Li
litianduo@163.com

¹ Shandong Provincial Key Laboratory of Molecular Engineering, School of Chemistry and Pharmaceutical Engineering, Qilu University of Technology, Jinan 250353, PR China

Graphical Abstract

Skeleton crystal is a special form of crystal crystallization. Rock salt structure is an important part of the formation of skeleton crystal. The growth rate of the edge of the NiO crystal is higher than that of the crystal surface, and the (111) plane decreases or even disappears, eventually forming a skeleton crystal NiO octahedral structure.



Highlights

- A special morphology of NiO skeleton crystal octahedron was synthesized by a one-step template-free method.
- The formation mechanism of surface depression NiO octahedron was explained based on the definition of skeleton crystal.
- The effect of surface depression on electrochemical performance is explained.

Keywords Electrochemical supercapacitors · NiO octahedron · Skeleton crystal · Depression

1 Introduction

In recent years, electrochemical supercapacitors have attracted great attention as a new type of energy storage device with a high power density and durability [1–3]. RuO_2 and IrO_2 are well studied as two kinds of pseudocapacitive capacitive electrode materials [4]. However, the use of these materials is limited by their high cost. Alternative materials such as NiOx [5–7], CoOx [8, 9], and MnO_2 [10, 11] have been made in various combinations to overcome cost factors. In these materials, NiO is usually used in rechargeable batteries and supercapacitors, which is due to its low cost, easy access, and comparable electrochemical behavior and high theoretical capacity (theoretical C_p of NiO is $\sim 2573 \text{ F g}^{-1}$ [12]). NiO nanostructure has the small particle size, large surface area, apparent quantum effect, and easy to adjust the surface microstructure in the nanometer scale. It is widely used in magnetic material [13], catalyst [14], battery electrode [15], and gas sensor [16] of inorganic materials. The regular shape of nanocrystalline metal oxide crystals is an important branch of research in the preparation of metal oxide supercapacitors. Mastery over their shape results in control over their properties and enhancement of their usefulness for a given application [17]. So far, many morphologies of NiO have been

prepared, such as nanospheres [18], nanorods [19], nanoflowers [20], nanotubes [21], nanowires [22], nanosheets [23], and nanopolyhedra [24]. Under normal circumstances, the preparation methods of nano-scale NiO octahedron include solvothermal and hydrothermal synthesis [25], chemical vapor deposition [24], sonochemical [26], and electrodeposition processes [27, 28]. So far, NiO octahedrons have been prepared by a variety of experimental methods. Liu et al. reported that NiO octahedral materials exposed (111) crystal faces have higher photocatalytic activity than P25 [29]. Yang et al. prepared the NiO octahedron with smooth surfaces. Electrochemical tests showed that the octahedral and agglomerated structures have high lithium storage capacity [30]. However, these methods usually involve multiple steps, stabilizers, organic solvents, and even template. Therefore, it is very important to find a simple, effective, and environmental-friendly synthetic strategy. To the best of our knowledge, NiO octahedrons with surface depressions skeleton crystal are rarely mentioned, despite some progress achieved in the synthesis of octahedron particles.

In this paper, we report a one-step and template-free method to synthesize NiO octahedrons. The NiO samples have been tested as supercapacitor electrode materials in 3.0 mol L^{-1} KOH electrolytes. We analyzed the mechanism

of the different morphogenesis of NiO crystals. The results of the electrochemical supercapacitor characteristics showed that the surface depression skeleton crystal NiO octahedron having fine supercapacitive behaviors and specific capacitance values at the discharging current of 0.5 A g⁻¹ is 640 F g⁻¹ in the 3 mol L⁻¹ KOH electrolyte and maintain excellent cycling stability, remaining constant after 2000 cycles. Electrochemical impedance measurements confirmed the capacitance performance of NiO electrodes.

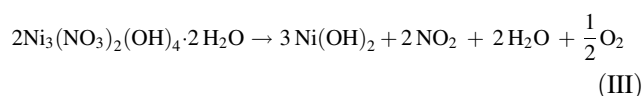
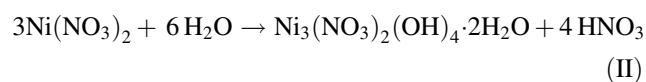
2 Experimental

2.1 Materials

Ni(NO₃)₂·6H₂O, anhydrous ethanol, and KOH were purchased from Shanghai Chemical Co. Reagent company. These were directly used as received without further purification. All other reagents are of analytical reagent grade, unless stated otherwise.

2.2 Preparation of the nickel oxide octahedral

The related thermal decomposition chemical reaction of the synthetic template-free skeleton crystal NiO octahedron can be summarized as follows:



In a typical experiment, 0.02 mol Ni(NO₃)₂·6H₂O was dissolved in 20 mL of anhydrous ethanol, and stirred at 30 °C for 0.5 h until the solution was completely dissolved. The solution was then transferred to the oven and heated to 110 °C for 8 h. The pale green precursor was recovered by filtration and washed repeatedly with deionized water and anhydrous ethanol to remove undecomposed impurities. Additionally, the samples were annealed at 400 °C for 2 h. In order to study the influence of temperature on the morphology, the original experimental conditions were kept constant, and the annealing temperature was adjusted to 600 and 800 °C, respectively. Finally, the samples were cooled to room temperature.

In order to study the effect of calcination time on the morphology of NiO, different samples were obtained at different times under the premise of calcining the precursors at 400 and 600 °C, respectively. They are labeled 400-0.5, 400-1, 400-1.5, 600-0.5, 600-1, and 600-1.5, respectively.

2.3 Electrochemical tests

Electrodes for electrochemical studies were prepared by mixing 80 wt% of the as-obtained NiO crystals, 10 wt% conducting acetylene black, and 10 wt% binder (polyvinylidene difluoride, PVDF). The prepared slurry was evenly coated on a nickel foam base with an area of about 1 cm² and then dried at 60 °C for 12 h as the working electrode. Electrochemical experiments were performed on an electrochemical workstation (PARSTAT 4000) using 3 mol L⁻¹ KOH as the electrolyte. Cyclic voltammetry functions using a three-electrode cell (a saturated calomel electrode (SCE) as the reference electrode, a Pt electrode as the counter electrode).

2.4 Characterization

X-ray diffraction patterns were recorded using a Bruker D8 advance X-ray diffractometer with Cu K α radiation (40 kV, 40 Ma, $\gamma = 0.15406$ nm). The diffraction data were collected at a scan rate of 2° min⁻¹ in the 2 θ range from 20° to 80°. The tube voltage and current were 40 kV and 40 mA, respectively. Scanning electron microscopy (SEM) was performed using an S-4800 Field Emission SEM (FESEM, Hitachi, Japan) at an accelerating voltage of 10 kV. Thermogravimetric (TGA) analyses were conducted using a Shimadzu TGA-50 (Shimadzu, Tokyo, Japan) analyzer with temperature programmed at a constant heating rate of 10.0 K min⁻¹ in air with a gas flow of 25 mL min⁻¹.

3 Results and discussion

3.1 XRD analysis of the samples

According to the Joint Committee on Powder Diffraction Standards (JCPDS) card no. 27-0939, the sample formed in Fig. 1a can be assigned to hexagonal structure Ni₃(NO₃)₂(OH)₂·2H₂O. The phase structures of the samples are clearly characterized by XRD patterns as shown in Fig. 1b, representing the X-ray diffraction spectra corresponding to the annealing temperatures of 400, 600, and 800 °C. The diffraction peaks located at 37.2°, 43.3°, 62.9°, and 75.4° can be well indexed to the (111), (200), (220), (311), and (222) crystal planes of cubic NiO (JCPDS card no. 47-1049) [31], respectively. It can be seen from Fig. 1b that the samples obtained after calcination have good crystallinity.

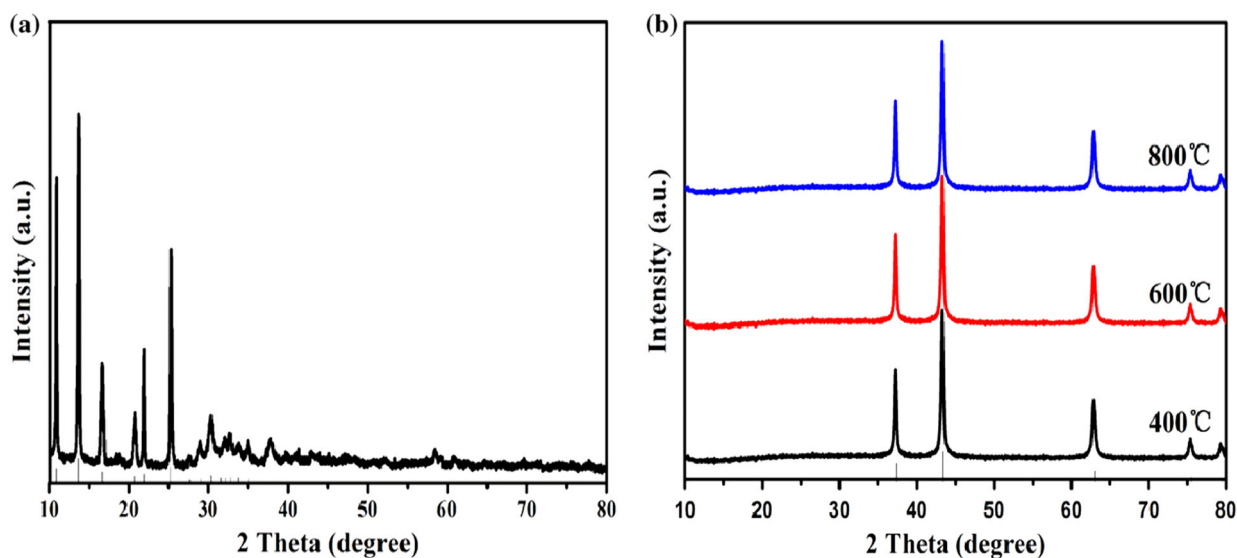


Fig. 1 XRD pattern of **a** nickel oxide precursor and **b** 400 °C, 600 °C, and 800 °C

Moreover, the diffraction peaks gradually strengthened. When annealing temperatures was 400 °C, the $I(200)/I(111)$ intensity ratio of the samples was 1.69, When the calcination temperature was 600 °C, the $I(200)/I(111)$ intensity ratio of the samples was 1.73, When the calcination temperature was 800 °C, the $I(200)/I(111)$ intensity ratio of the samples was 1.96. In the present study, $I(200)/I(111)$ underwent a linear increase from 400 to 800 °C, suggesting an enhancement in the anisotropy of NiO octahedral particles [32]. No characteristic peaks of impurities were detected in the XRD patterns.

3.2 Thermogravimetric analysis

The TGA curve (Fig. 2) analysis showed that the precursor NiO decomposed at about 400 °C. As shown in Fig. 2, the precursor TGA curve showed about 50% weight loss from 25 to 850 °C. This weight loss can be roughly divided into three stages. The first stage involved a weight loss of about 10% below 200 °C, which mainly due to the desorption of surface-absorbed H₂O. The second stage involved a dramatic weight loss of ~7% between 200 and 270 °C, which due to the decreasing of the bound water of the sample. The third stage involved ~33% weight loss between 270 and 390 °C, due to the decomposition of oxygen-containing groups. The weight of the sample continuously decreases up to ~390 °C, after which no obvious weight loss is further observed. It can be seen from the thermogravimetric curve that the precursor decomposed after 390 °C, so we chose 400, 600, and 800 °C as the calcination temperature to prepare the NiO samples. The TGA analysis curve showed

that there is no significant weight loss in the NiO samples (400, 600, and 800 °C). This is consistent with the conclusions drawn from the precursor TGA curve.

3.3 SEM analysis of the samples

A representative field-emission scanning electron microscopy (FESEM) image of NiO calcined sample at 400 °C for 2 h is shown in Fig. 3a, b. It can be seen from Fig. 3b that the NiO octahedron consists of 8 equilateral triangular surfaces and 12 identical edges (average side length of 300–500 nm). The NiO has a good octahedral structure, but it can be found that there are many small depressions on the surface of the NiO octahedron after calcination.

When the calcination temperature was changed to 600 °C, the morphology of NiO remains an octahedron structure, but it is different from the previous octahedron. As shown in Fig. 3c, d, the shape of the product is relatively simple, and the size of the single crystal is more regular. The size of the product is about 500 nm. These NiO crystals have the characteristics of coarse crystal edges, depression surface, and obvious triangular holes.

When the annealing temperature is up to 800 °C, the morphologies of the products are shown in Fig. 3e. The morphology of NiO is no longer octahedron structure, but a small square. As shown in Fig. 3f, the diameter of a square block is about 200 nm, and the edge of the crystal is clear. Therefore, the morphology and structure of NiO can be optimized by controlling the annealing temperature in a certain range.

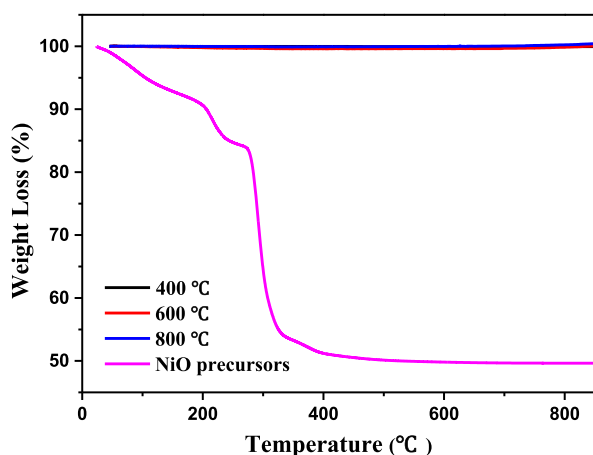


Fig. 2 TGA profiles of NiO precursor (heating rate = $10\text{ }^{\circ}\text{C min}^{-1}$ under the air atmosphere)

3.4 Electrochemical behavior of NiO octahedral

In order to explore the potential advantages of the samples as an energy storage device, the synthesized samples were made into supercapacitor electrodes. The electrochemical performance of NiO octahedrons was evaluated in 3 mol L^{-1} KOH electrolyte solution using a three-electrode system in the potential range 0.1–0.4 V. EIS, CV, and GCD measurements were performed to compare the properties of these materials.

In order to verify the electrochemical properties of the prepared electrode materials, EIS was used to characterize the sample. EIS is an effective method to measure the electronic conductivity in the redox process. As shown in Fig. 4a, the slope of 600 °C sample is larger than that of the other two samples in the low-frequency region, indicating that it has the lowest impedance. Because it has the lowest impedance, it can be concluded that 600 °C sample has the best electrochemical performance. Figure 4b shows the CV curves of the NiO ranging from 5 to 100 mV s^{-1} at different scan rates. With the increasing scanning speed, the shape of CV curve is maintained, demonstrating that the NiO modified working electrode exhibits satisfactory rate and cycle performance [33]. Figure 4c shows a pair of cathodic and anodic peaks in the CV curves for all three samples at different scan rates. One peak is anodic (positive current density) during the oxidizing reaction of Ni^{2+} to Ni^{3+} , and the other is cathodic (negative current density) during the reverse process. The anodic peak in the CV profile shifted towards positive potentials with an increase in the scan rate and the cathodic peak to the negative potential on account of the polarization in the electrode material [34]. These peaks are derived from the rapid reversible redox process on the surface of the electrode, according to the following

equation [35]:



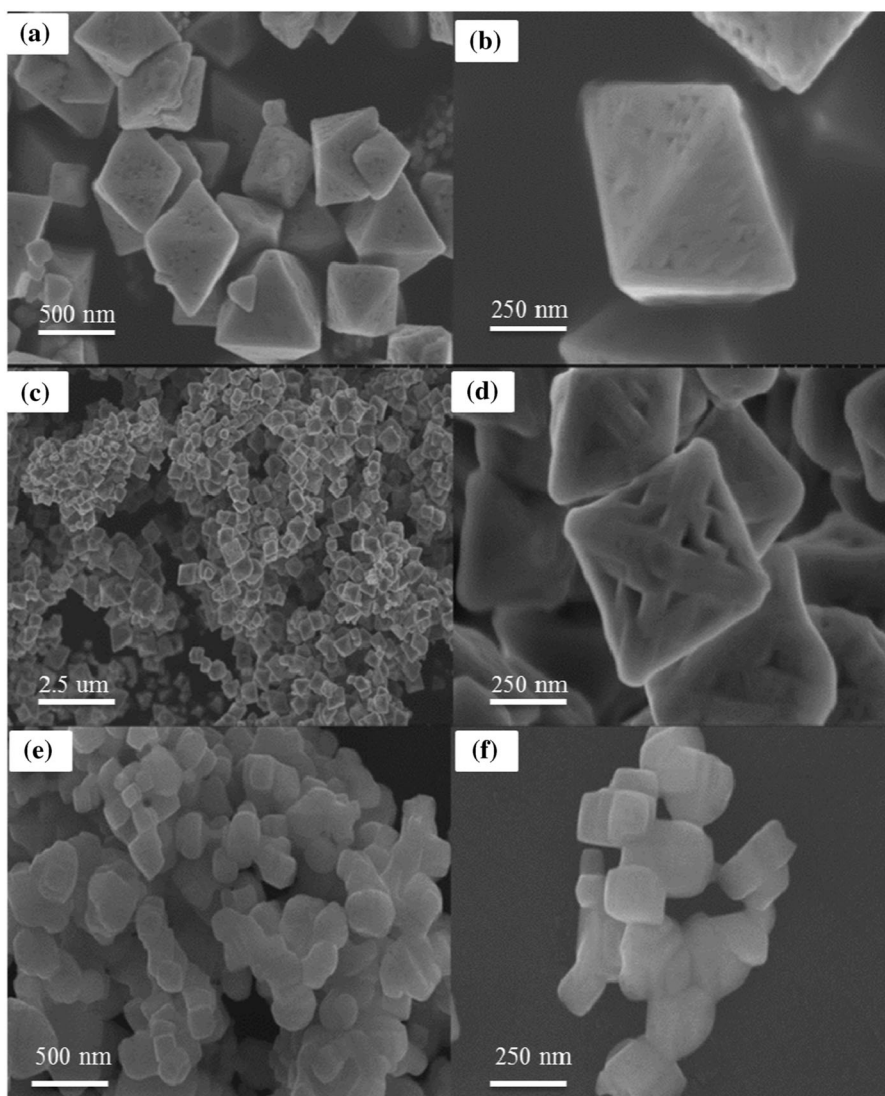
The cathode peak and anode peak position changed slightly with the increasing of scanning rate, which indicated that the electrochemical reaction speed is fast, and the electrode resistance is generated during redox reaction. The redox peak can be observed at all scanning rates, which is mainly due to the different conversion of nickel between redox states [35, 36]. Therefore, the specific capacitance is improved by making full use of the electroactive surface of NiO particles at low scanning rate. The decrease in specific capacitance is attributed to the NiO nanostructure which cannot sustain the redox reactions at a higher current. Figure 4d shows that the GCD curves of the NiO samples are tested at current density of 0.5 A g^{-1} from 0 to 0.4 V using 3.0 mol L^{-1} KOH solution as the electrolyte. All of the non-linear charge–discharge curves confirmed the tantalum capacitor properties of the NiO electrode, which is consistent with the CV results. Obviously, each curve with a clear platform corresponds to the Faraday discharge process. For the three-electrode cell, the specific capacitance of the electrode was calculated using GCD curves [37]:

$$C = \frac{I\Delta t}{m\Delta V} \quad (1)$$

where C is the specific capacitance (F g^{-1}), I is the discharge current (A), m is the mass of the electrode (g), ΔV is the potential window (V), and Δt is the total discharge time (s). The specific capacitance values obtained from charge–discharge studies are 350, 640, and 110 F g^{-1} for 400, 600, and 800 °C samples electrodes at a current density of 0.5 A g^{-1} . The significant increase in specific capacitance of the 600 °C sample is mainly attributed to its depression structure, which provides effective diffusion channels for electrolyte ions, resulting in improved pseudocapacitance performance. In particular, this porous nanostructure can act as an “ion buffer reservoir” [38], maintaining the supply of OH^{-} and ensuring that a sufficient Faradaic reaction can be stored at high current densities.

Cycling stability performance is another important parameter of the electrochemical supercapacitor. Figure 5 illustrates specific capacitance retention as a function of cycle number based on the CV curves at a current density of 20 mV s^{-1} of NiO (600 °C). The specific capacitance increased by about 8% for the three types of NiO during the first 50 cycles, which is possibly due to the activation process of the NiO electrodes [39]. As the scanning process continues, the specific capacitance of the NiO octahedron crystal at 600 °C, remains stable, which confirms stable

Fig. 3 SEM images of **a** 400 °C, **c** 600 °C, and **e** 800 °C (**b**, **d**, and **f** are the partial magnification of **a**, **c**, and **e**, respectively)



cycle performance and high Coulombic efficiency. Besides, these values are higher than those obtained from other NiO powder materials. The morphology, synthesis method, and electrochemical performance of as-obtained NiO and other electrodes are provided for comparison, as shown in Table S1. It can be concluded, this higher capacitance retention implies that the depression NiO octahedron is a suitable material for supercapacitor application.

3.5 Formation mechanism of the NiO samples

For the study of the formation of NiO octahedron, time-dependent growth experiments were performed. Figure S1 shows the XRD images of 400-0.5 h, 400-1 h, and 400-1.5 h. Undoubtedly, the three samples are all pure NiO (JCPDS card no. 47-1049) based on their XRD patterns. Figure S2 shows SEM patterns of NiO precursor, 400-0.5 h, 400-1 h,

and 400-1.5 h. It can be seen from the SEM that the morphology of the samples changes significantly with the calcination time. Figure S2a shows the SEM of the precursor with irregular nanoparticle morphology. The nanoparticles ($\text{Ni}_3(\text{NO}_3)_2(\text{OH})_2 \cdot 2\text{H}_2\text{O}$, diameter: 50–100 nm) are prone to agglomeration. When the calcination time was 0.5 h, small NiO octahedron and unformed particles were formed by sintering $\text{Ni}_3(\text{NO}_3)_2(\text{OH})_2 \cdot 2\text{H}_2\text{O}$ (Fig. S2b). When the sintering time was increased to 1 h, the small octahedron was further grown to have a side length of about 100 nm (Fig. S2c). By further increasing the sintering time to 1.5 h, many particles having an octahedral structure (side length: 250–500 nm) were observed, as shown in Fig. S1d. At the final stage of formation (2 h), the octahedral particles became larger and more uniform in shape, but the surface of the sample became relatively rough (Fig. 3a, b). The observations provide the first direct evidence that the octahedral NiO structures undergo a continuous transformation from

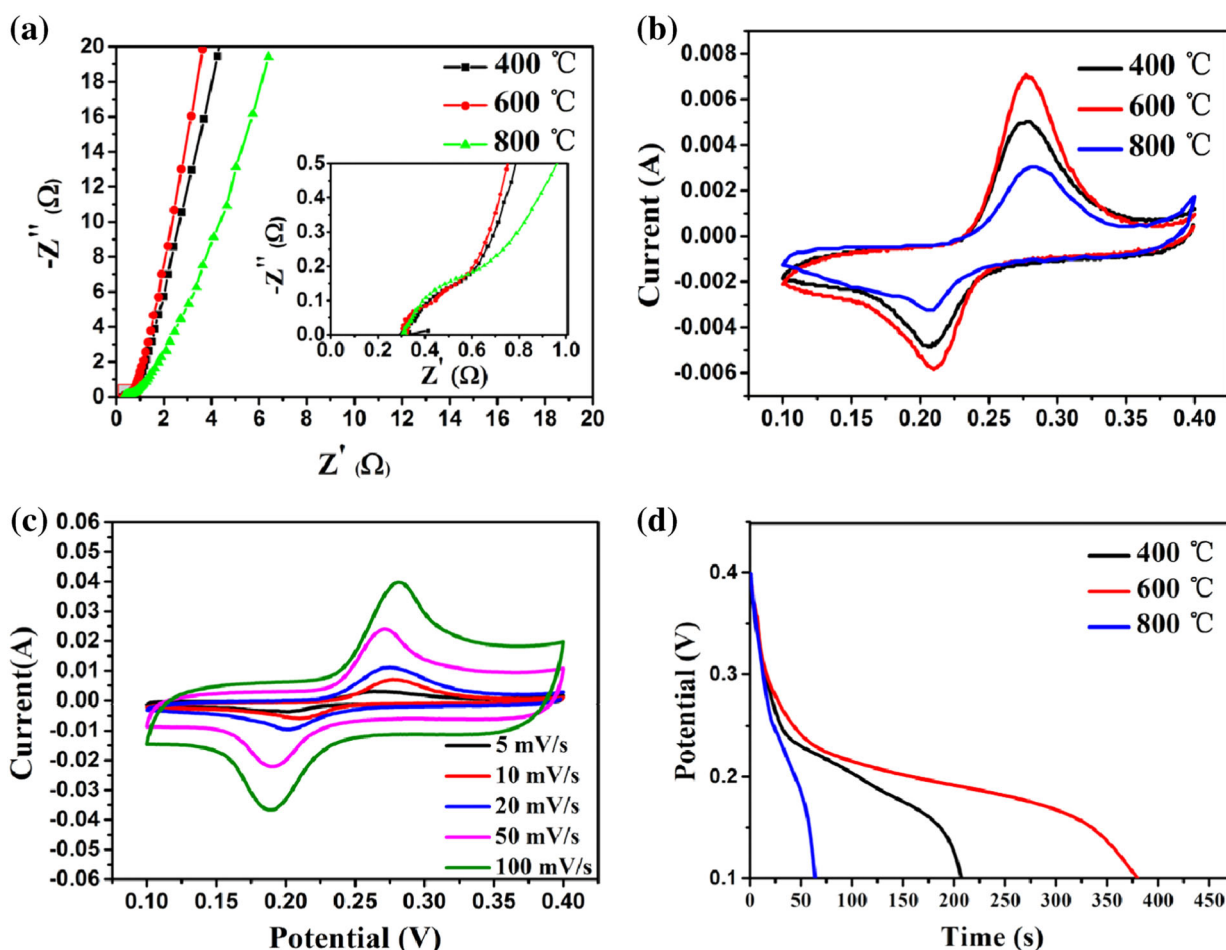


Fig. 4 **a** Nyquist plots of 400 °C, 600 °C, and 800 °C, **b** CV curves of 400 °C, 600 °C, and 800 °C at the scan rate of 10 mV s⁻¹, **c** CV curves of the 600 °C at different scan rates (5, 10, 20, 50, and 100 mV s⁻¹), **d** GCD curves of 400 °C, 600 °C, and 800 °C

irregular particles to small octahedra and then to large octahedra with increasing sintering time, as illustrated in Fig. S2. This implies an important role of calcination time in the production of octahedral NiO structures.

For the study of the formation of NiO skeleton crystal octahedron, time-dependent growth experiments were performed. The XRD patterns in Fig. 6a show that the products formed from 0.5 to 1.5 h are pure face-centered cubic (FCC) phases of NiO (JCPDS card no. 47-1049). Moreover, the diffraction peaks gradually strengthened, and the $I(200)/I(111)$ intensity ratio of the samples was enhanced from 1.53 to 1.56 with increasing time from 0.5 to 1.5 h. It can be seen from Fig. 6b that the NiO octahedron (111) face becomes rough and has some small depressions at 600 °C for 0.5 h. It can be seen from Fig. 6c, when the calcination time was increased to 1 h, the depression of the (111) plane of the NiO octahedron is further enlarged compared with the coarse depression. As can be seen from Fig. 6d, the surface of the sample was relatively smooth but the dents became more pronounced as the calcination time was increased to

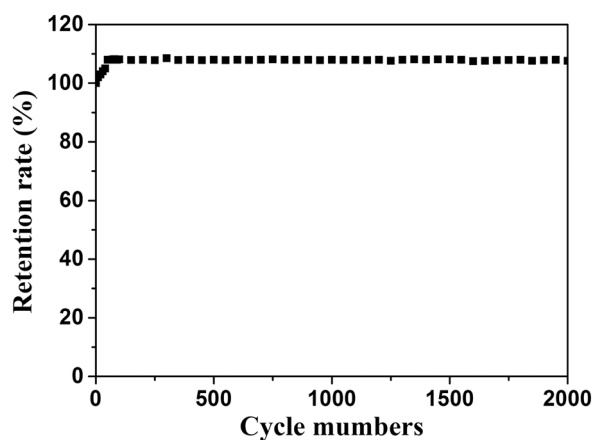


Fig. 5 Cycle stability of 600 °C measured at a scan rate of 20 mV s⁻¹ of the CV curves

1.5 h. When the final calcination time was 2 h, it was seen from Fig. 3d that some of the NiO octahedron (111) faces were completely recessed to form a skeleton crystal NiO octahedron. Time-dependent structural evolution (NiO

Fig. 6 **a** XRD patterns and SEM images of NiO samples obtained by calcining the NiO precursors at 600 °C for different times: **b** 0.5 h, **c** 1 h, **d** 1.5 h

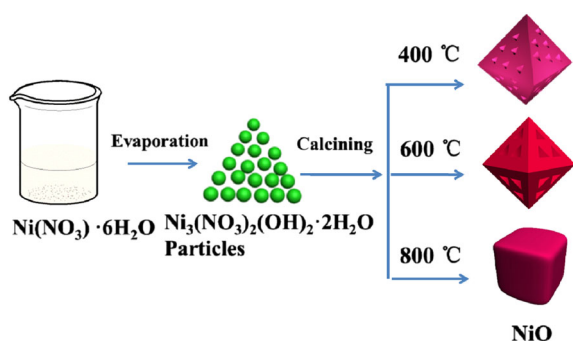
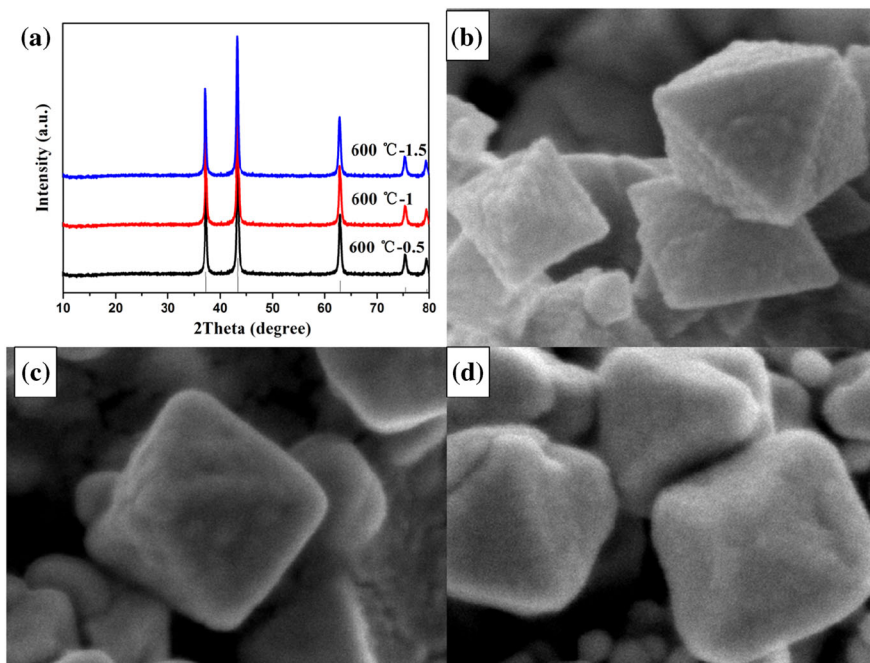


Fig. 7 Formation mechanism of the NiO octahedron

octahedral particles) and alteration (skeleton crystal NiO octahedral morphology) strongly suggested that sintering time can be used as a tool to control the growth process of three-dimensional structures. They can be used as intermediates in the final product: experiments have shown that the formation of skeleton crystal NiO octahedral structures is indeed related to the preparation conditions.

Figure 7 shows that the synthesis process and schematic diagram of NiO octahedron. The light green $\text{Ni}_3(\text{NO}_3)_2(\text{OH})_2 \cdot 2\text{H}_2\text{O}$ precursor was formed via a one-pot reaction and then synthesized NiO after calcination at different temperatures. $\text{Ni}_3(\text{NO}_3)_2(\text{OH})_2 \cdot 2\text{H}_2\text{O}$ actually corresponds to $\alpha\text{-Ni}(\text{OH})_2$ with a hydrotalcite-like structure and composed of laminated $\text{Ni}(\text{OH})_{2-x}$ layers with NO_3^- and water molecules in the interlayer [40]. At around 300 °C (Fig. 2), the mass of the precursor decreased rapidly. This was attributed to the decomposition of NO_3^- to NO_2 , in which the precursor became $\alpha\text{-Ni}(\text{OH})_2$, and the melting

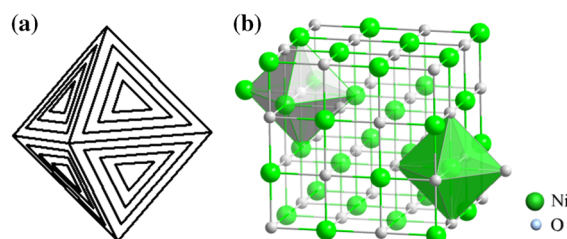


Fig. 8 **a** Rock salt skeleton crystal (funnel shape) and **b** atomic array diagram of NiO

point of $\alpha\text{-Ni}(\text{OH})_2$ is 230 °C. Therefore, when the calcination temperature is higher than the melting point of the sample, $\alpha\text{-Ni}(\text{OH})_2$ will be in a molten state. Then, the crystals recrystallized when the samples were cooled to room temperature. Generally, FCC crystals have a general surface energy sequence, $\gamma(111) < \gamma(100) < \gamma(110)$ [41, 42]. According to the principle of minimum surface free energy, nanoparticles usually have to be surrounded by crystal planes of lower energy. In this case, the precursor forms a (111) FCC phase of NiO formed by a triangle during the melt recrystallization process. When the precursor was calcined at 400 °C, in the process of rapid growth with only diffusion mechanism, the crystal interface will show instability when nucleating in the liquid region near the gas–liquid interface. At the same time, due to austenitic ripening, the grains on the surface of the crystal will combine with each other to form large particles, resulting in some small depressions on the surface. When the precursor was calcined at 600 °C, the NiO octahedron formed has a larger depression on the surface than the NiO octahedron

formed at 400 °C. Because during the crystallization of the NiO octahedron, the growth conditions of the skeleton crystals are satisfied as the temperature increases. Skeleton crystal is a special form of crystal crystallization. When the solution is extremely supersaturated, the crystallization speed rate is fast and the viscosity of the system is large, the crystal lattice of the crystal develops very fast, and the crystal plane is hardly developed. Most of the crystals no longer have a chance to be filled in the later stage, so that a funnel is formed in the middle of the crystal faces to form skeletal structures. Rock salt structure is an important part of the formation of skeleton crystal. Figure 8a shows the theoretical diagram of rock salt skeleton crystal (funnel shape). NiO is the rock salt structure as shown in Fig. 8b. Both Ni²⁺ and O²⁻ are octahedral type coordination, and the whole crystal can be regarded as a FCC arrangement of Ni and O. The growth rate of the edge of the NiO crystal is higher than that of the crystal surface, and the (111) plane decreases or even disappears, eventually forming a skeleton crystal NiO octahedral structure [43]. As the calcination temperature increases, the crystal morphology tends to be isotropic [32]. Therefore, the crystal is no longer an octahedron but a cube, and the surface is composed of a mixture of (100) and (111) faces. When the precursor is calcined at 800 °C, an excessively high calcination temperature not only provides the energy required for decomposition, but also increases the rate of crystal nucleation. The rate of nucleation increases faster than nucleus, so that smaller grains can be obtained [32]. Obviously, the above results show that the structure and morphology of the obtained NiO product strongly depend on the decomposition temperature of Ni(NO₃)₂·6H₂O.

4 Conclusion

In summary, three different topographies were prepared by calcination at different temperatures. In electrochemical tests, surface depression skeleton crystal NiO octahedron showed stable cycling performance with high specific capacitance. The formation of surface depression by recrystallization at 600 °C calcination is a key factor for good electrochemical performance. The formed surface depression provided effective diffusion channels for electrolyte ions, resulting in improved pseudocapacitance performance. In particular, surface depression structure can act as “ion buffers” to maintain the supply of OH⁻ and ensure that a complete Faraday reaction can be stored at high current densities. When surface depressed NiO octahedron is tested as an electrode of a supercapacitor, the specific capacitance is much higher than that of the octahedron and the cube. This approach also provides a potential strategy to

improve the performance of supercapacitors made from a variety of other materials.

Acknowledgements This study was supported by the financial support of the Key Research Project of Shandong Province (No. 2017GGX40121), the National Natural Science Foundation of China (Nos. 51402157 and 51602164), and the Scientific Research Innovation Team in Colleges and Universities of Shandong Province.

Compliance with ethical standards

Conflict of interest The authors declare that they have no conflict of interest.

Publisher's note: Springer Nature remains neutral with regard to jurisdictional claims in published maps and institutional affiliations.

References

- Pandolfo AG, Hollenkamp AF (2006) *J Power Sources* 157:11–27
- Yang Z, Zhang J, Kintner-Meyer MC, Lu X, Choi D, Lemmon JP, Liu J (2011) *Chem Rev* 111:3577
- Chen G, Guan H, Dong C, Wang Y (2017) *Ionics* 24:513–521
- Hu CC, Chang KH, Lin MC, Wu YT (2006) *Nano Lett* 6:2690
- Inamdar AI, Kim YS, Pawar SM, Kim JH, Im H, Kim H (2011) *J Power Sources* 196:2393–2397
- Wu M, Gao J, Zhang S, Chen A (2006) *J Porous Mater* 13:407–412
- Dhole IA, Navale ST, Navale YH, Jadhav YM, Pawar CS, Suryavanshi SS, Patil VB (2017) *J Mater Sci Mater Electron* 28:10819–10829
- Pang M, Yuan JI (2014) Solvothermal synthesis of CoO spheres and their excellent electrochemical performances in supercapacitors. In: Proceedings of the national energy storage science and technology conference
- Liu X, Ji D, Li J, Chen L, Zhang D, Liu T, Zhang N, Ma R, Qiu G (2015) *RSC Adv* 5:41627–41630
- Ghodbane O, Pascal JL, Favier F (2009) *ACS Appl Mater Interfaces* 1:1130
- Yu P, Zhang X, Wang D, Wang L, Ma Y (2013) *Cryst Growth Des* 9:528–533
- Nam KW, Kim KB (2002) *J Electrochem Soc* 149:A346–A354
- Tiwari S, Rajeev K (2006) *Thin Solid Films* 505:113–117
- Nohman AKH, Mekhemer GAH, Tolba MA (2003) *Bull Fac Sci Assuit Univ* 32:1–11
- Raza R, Liu Q, Nisar J, Wang X, Ma Y, Zhu B (2011) *Electrochem Commun* 13:917–920
- Predanoc M, Hotový I, Řehaček V (2017) Gas sensor based on sputtered NiO thin films. In: Proceedings of the international conference on advanced semiconductor devices & microsystems
- Fan X, Guan J, Li Z, Mou F, Tong G, Wang W (2010) *J Mater Chem* 20:1676–1682
- Chen J, Wu X, Liu Y, Gong Y, Wang P, Li W, Mo S, Tan Q, Chen Y (2017) *Appl Surf Sci* 425:461–469
- Li Q, Huang G, Yin D, Wu Y, Wang L (2016) *Part Part Syst Charact* 33:764–770
- Chai H, Chen X, Jia D, Bao S, Zhou W (2012) *Mater Res Bull* 47:3947–3951
- Cao F, Pan GX, Xia XH, Tang PS, Chen HF (2014) *J Power Sources* 264:161–167
- Vidhyadharan B, Zain NKM, Misnon II, Aziz RA, Ismail J, Yusoff MM, Jose R (2014) *J Alloy Compd* 610:143–150

23. Zhang Q, Liu H, Li H, Liu Y, Zhang H, Li T (2015) *Appl Surf Sci* 328:525–530
24. Chen DP, Wang XL, Du Y, Ni S, Chen ZB, Liao X (2012) *Cryst Growth Des* 12:2842–2849
25. Meher SK, Justin P, Rao GR (2010) *Electrochim Acta* 55:8388–8396
26. Song X, Lian G (2008) *J Am Ceram Soc* 91:3465–3468
27. And RN, Elsayed MA (2005) *ChemInform* 109:12663–12676
28. Zecchina A, Groppo E, Bordiga S (2010) *Chemistry* 13:2440–2460
29. Liu B, Wei A, Zhang J, An L, Zhang Q, Yang H (2012) *J Alloy Compd* 544:55–61
30. Yang ZK, Song LX, Xu RR, Teng Y, Xia J, Zhao L, Wang QS (2014) *CrystEngComm* 16:9083–9089
31. Liu B, Yang H, Wei A, Zhao H, Ning L, Zhang C, Liu S (2015) *Appl Catal B: Environ* 172–173:165–173
32. Tong G, Hu Q, Wu W, Li W, Qian H, Liang Y (2012) *J Mater Chem* 22:11754–17494
33. Gujar TP, Kim WY, Puspitasari I (2007) *Int J Electrochem Sci* 2:666–673
34. Qing X, Liu S, Huang K, Lv K, Yang Y, Lu Z, Fang D, Liang X (2011) *Electrochim Acta* 56:4985–4991
35. Hu CC, Chang KH, Hsu TY (2008) *J Electrochem Soc* 155:196–200
36. Srinivasan V, Weidner JW (2000) *J Electrochem Soc* 147:880–885
37. Kaempgen M, Chan CK, Ma J, Cui Y, Gruner G (2009) *Nano Lett* 9:1872
38. Wang DW, Li F, Liu M, Lu GQ, Cheng HM (2010) *Angew Chem* 120:379–382
39. Yuan C, Zhang X, Su L, Gao B, Shen L (2009) *J Mater Chem* 19:5772–5777
40. Liu BH, Yu SH, Chen SF, Wu CY (2006) *J Phys Chem B* 110:4039–4046
41. Niu W, Zheng S, Wang D, Liu X, Li H, Han S, Chen J, Tang Z, Xu G (2009) *J Am Chem Soc* 131:697–703
42. Xiong YJ, Wiley BJ, Xia Y (2010) *Angew Chem* 46:7157–7159
43. Jin W, Cai L, Pan Z, Miao Y (2000) *J Inorg Mater* 15:769–776